Innovative Systems Design and Engineering
ISSN 2222-1727 (Paper) ISSN 2222-2871 (Online)
Vol 2, No 4, 2011

Dynamic Modeling of Chatter Vibration in Cylindrical Plunge Grinding Process

Samuel Karanja Kabini (Corresponding Author)
Department of Mechatronic Engineering
Jomo Kenyatta University of Agriculture and Technology
P.O. Box 62000-00200, Nairobi, Kenya
Tel. +254 720 980 179, Email: kkabini@eng.jkuat.ac.ke

Dr. Bernard Wamuti Ikua
Dean
School of Mechanical, Manufacturing and Materials Engineering
Jomo Kenyatta University of Agriculture and Technology
P.O. Box 62000-00200, Nairobi, Kenya
Tel. +254 722 286 264, Email: ikua_bw@eng.jkuat.ac.ke

Dr. George Nyauma Nyakoe
Head
Department of Mechatronic Engineering
Jomo Kenyatta University of Agriculture and Technology
P.O. Box 62000-00200, Nairobi, Kenya
Tel. +254 721 4 56 661, Email: nyakoe@eng.jkuat.ac.ke

The research is financed by Jomo Kenyatta University of Agriculture and Technology

Abstract
Cylindrical plunge grinding process is a machining process normally employed as a final stage in precision machining of shafts and sleeves. The occurrence of chatter vibrations in cylindrical plunge grinding limits the ability of the grinding process to achieve the desired accuracy and surface finish. Moreover, chatter vibration leads to high costs of production due to tool breakages.

In this paper, a theoretical model for the prediction of chatter vibration in cylindrical grinding is developed. The model is based on the geometric and dynamic interaction of the work piece and the grinding wheel. The model is validated with a series of experiments. Results show that variation in the grinding wheel and work piece speeds, and in-feed lead to changes in the vibration modes and amplitudes of vibration.

Keywords: Cylindrical, plunge, grinding, process, chatter, vibration, kinematics, modeling.

1. Introduction

Cylindrical plunge grinding process is inherently susceptible to chatter vibration owing to the grinding wheel-work piece interaction (Inasaki 1999, Franciszek 1999). Occurrence of chatter vibrations during the grinding

process has detrimental effects on accuracy and surface finish of the machined part, (Hongqi 2007, Garitaonandia 2010).

With a comprehensive dynamic model of the grinding process, chatter vibration can be predicted and its occurrence prevented, by use of a process controller. Modeling of the grinding process can be achieved through development of either empirical or theoretical models. It generally involves a trade-off between the accuracy of the model and the difficulty in obtaining the necessary information or parameters (Daniel 1999).

In recent years, many researchers have attempted to develop models for the grinding process. This has resulted in a large number of models for the grinding process, each attempting to look at, or emphasize on, a specific area of the grinding processes.

Theoretical grinding models for calculating material removal are based on the specific cutting energy of the material and energy distribution of the applied power (Merchant 1945). Rogelio and Steven (2006) developed the equations governing surface roughness for plunge grinding. The equations included several physical mechanisms in grinding such as wheel-work piece overall deflection, local grit deflection and individual grit-work piece interaction.

Similar work was reported (Piotr 2007), where a simulation model of the grinding process for regular surface texture generation was developed. The model assumed random arrangement of abrasive grains. The verification of the model was carried out through measurements of grinding force.

Some work was carried out (Mohammed and Abdallah 2000), where the effects of dynamic changes in the grinding force components due to changes in the profile of the grinding wheel, and the work piece material on the vibration behavior of the grinding spindle were investigated. Biera and Nieto (1997) presented a time-domain dynamic model of the external plunge grinding process which consisted of a block-based simulation tool. Since the model was in time-domain non-linear effects could be considered. The model included the interference phenomenon between two consecutive work piece revolutions. Orynski and Pawlowski (1999) also conducted theoretical analysis of the dynamics for the machine tool-work piece system, for cylindrical plunge grinding process. A functional mathematical model for the grinder equipped with hydrostatic bearing on the grinding wheel spindle and hydrostatic slide ways was developed.

Orynski and Pawlowski (2002) developed a physical model of a cylindrical plunge grinder with hydrostatic slide ways and hydrostatic bearings for the grinding wheel spindle. The model was developed in order to investigate the influence of the grinding process on damping of forced vibration by the grinding wheel headstock. Huang and Wang (2008) presented a closed form expression for the stochastic grinding force as a function of the grinding conditions and grit distribution. The stochastic grit density function was introduced to describe the random grit distribution of the rotating wheel. The dynamic grinding force was formulated as the convolution of a single-grit force and the grit density function.

Sakakura et al (2004) carried out a visual simulation of the grinding process. The work involved several computer simulations using the Monte Carlo Method. Most of the simulations calculated static geometrical interference between a grain and a work piece. They also developed a simulation program based on the elastic behaviour model of a grain that focused on the generation process of a work piece surface, and simulation of the interaction of grains with a work piece, which includes the elastic and plastic deformation as well as the removal of work piece material.

Kuang and Wang (1997) modeled and predicted the grinding force for the creep feed grinding process, using back propagation (BP) neural network. The BP neural network was improved by integrating an error distribution function (EDF), to overcome local minimum problems. This was done in order to find the global minimum solution, and to accelerate the convergence speed.

From these works, there has been little attempt to develop a model for the prediction chatter vibrations in cylindrical plunge grinding process. This paper, presents a dynamic model for the prediction of chatter vibrations in cylindrical plunge grinding process.

2. Occurrence of chatter in cylindrical plunge grinding

Chatter vibration occurs when there is contact and relative motion between the grinding wheel and the work piece. It starts as a slip-slide interaction between wheel and work piece, and then causes the regenerative

effect, which is produced when the tool passes through a previously cut surface. The waves generated on the work piece surface are caused by the periphery of the grinding wheel and vice versa (Yi et al 2000). Certain conditions can cause the amplitudes of the relative vibration and the waves generated on the work piece surface to be identical. The conditions are; low vibration frequency, small relative amplitude and low work piece velocity (Ichiro 2008).

Under certain cutting conditions, the regeneration effect causes undulations of the work piece to regenerate, leading to chatter vibrations, (Garitaonandia et al 2010). Chatter is caused by a number of factors that include: (i) *a heavy cut*, (ii) *non-uniformity of the work piece profile*, (iii) *change of material properties, which could be as a result of cast materials or hardening of the material being ground* and (iv) *too much or too low feed rate* (Hahn and Robert 1986).

There occurs relative vibrations to the waviness, and as the vibrations increase, the amplitude of waves generated on the work piece surface becomes smaller than that of the relative vibration. In other words, the envelope curve starts to have a mode (a characteristic pattern or shape in which the system will vibrate) (Junkar and Filipic 2001). Vibrations in cylindrical grinding affect the quality of the finished surface, the roundness of the work piece, and also the lifetime of the machine and the tool, (Lizarralde et al 2006).

3. Dynamic model of the cylindrical grinding process

In the dynamic model, chatter vibration is assumed to be a two dimensional problem as shown in Figure 1. In this figure, the radii of the grinding wheel and work piece are denoted as R_g and R_w respectively. A coordinate system that depends on the instantaneous positions of the grinding wheel and the work piece is used, X and Y being two orthogonal axes.

During the grinding process, the coordinate system is displaced (rotated) to the X' and Y' positions for the X and Y axes respectively. The displacement along the X axis is indicated as $(X_g - X_w)$, while that along the Y axis is indicated as $(Y_g - Y_w)$. The rotational speeds for the work piece and the grinding wheel are Ω_w and Ω_g respectively. β_w represents the angular position for the work piece and β_g shows the angular position for the grinding wheel. ψ is the angular displacement of the grinding wheel relative to the fixed work piece coordinate system, herein referred to as phase shift. After an in-feed f, the following relationship holds for the displacement in the x direction;

$$(X_g - X_w) = \{R_w \sin(\beta_w - \psi) + R_g \sin(\beta_g - \psi) - ft\} \cos\psi \quad (1)$$

For small β, $\sin\beta \approx \beta$, hence,

$$(X_g - X_w) \approx \{R_w(\beta_w - \psi) + R_g(\beta_g - \psi) - ft\} \cos\psi \quad (2)$$

Also, for the displacement in the y direction, the following relationship holds,

$$(Y_g - Y_w) \approx R_g(\beta_g - \psi) + R_w(\beta_w - \psi) - ft\} \sin\psi \quad (3)$$

Differentiation of eqns. 2 and 3 with respect to time yields the velocity terms in both the X and Y directions respectively;

$$(\dot{X}_g - \dot{X}_w) = \{R_g(\Omega_g - \dot{\psi}) + R_w(\Omega_w - \dot{\psi}) - f\} \cos\psi - \{R_w(\beta_w - \psi) + R_g(\beta_g - \psi) - ft\} \sin\psi \quad (4)$$

$$(\dot{Y}_g - \dot{Y}_w) = \{R_g(\Omega_g - \dot{\psi}) + R_w(\Omega_w - \dot{\psi}) - f\} \sin\psi - \{R_w(\beta_w - \psi) + R_g(\beta_g - \psi) - ft\} \cos\psi \quad (5)$$

The phase shift ψ can be obtained from the following geometric relation,

$$R_g + R_w = R_g(\beta_g - \psi) + R_w(\beta_w - \psi) \quad (6)$$

from which the expression for ψ becomes;

$$\psi = \frac{R_g\beta_g + R_w\beta_w - R_g - R_w}{R_g + R_w} \quad (7)$$

The instantaneous velocity terms v_t and v_n in the tangential and normal directions respectively, will be given as;

$$v_t = \Omega_w R_w (\beta_w - \psi) + (\dot{x}_g - \dot{x}_w) \times \sin\psi - (\dot{y}_g - \dot{y}_w)\cos\psi \quad (8)$$

$$v_n = -(\dot{x}_g - \dot{x}_w)\cos\psi + (\dot{y}_g - \dot{y}_w)\sin\psi \quad (9)$$

The dynamic model for the cylindrical plunge grinding process assumes distributed force along the wheel/work piece contact. The contact length along the wheel can be discretized into segments, each segment corresponding to a wheel angular increment $\Delta\beta$, as shown in Figure 2. The normalized instantaneous chip thickness, C_t can be given as, Hongqi and Shin (2007);

$$C_t = 2\pi \frac{V_t}{\Omega_g} \sin\Delta\beta_{gi} + 2\pi \frac{V_n}{\Omega_g} \cos\Delta\beta_{gi} \quad (10)$$

The specific segment forces per unit width of each contacted segment in radial and tangential directions can be represented as functions of the normalized chip thickness, C_t in the form;

$$\begin{pmatrix} f'_n \\ f'_t \end{pmatrix} = \begin{pmatrix} K_n \\ K_t \end{pmatrix} C_t(R_g \Delta\beta_{gi}) \quad (11)$$

The constants K_n and K_t are the normalized force coefficients for the radial and tangential directions respectively. The total specific segment forces in the normal and tangential directions can be obtained by summing up the segmental forces in the respective directions, i.e.,

$$\begin{pmatrix} F'_n \\ F'_t \end{pmatrix} = \sum_{i=1}^{N} \begin{pmatrix} K_n \\ K_t \end{pmatrix} C_t(R_g \Delta\beta_{gi}) \quad (12)$$

where

$$N = int\left(\frac{\beta_g}{\Delta\beta_{gi}}\right)$$

The total specific grinding forces F_n and F_t in the X and Y directions can be calculated by transforming the total segment forces, F'_n and F'_t in the Cartesian coordinate system i.e.,

$$\begin{pmatrix} F_n \\ F_t \end{pmatrix} = \begin{bmatrix} \cos(\beta_g + \psi) & -\sin(\beta_g + \psi) \\ \sin(\beta_g + \psi) & \cos(\beta_g + \psi) \end{bmatrix} \begin{pmatrix} F_n \\ F_t \end{pmatrix} \quad (13)$$

where F'_n and F'_t are given in equation 12. The values of F'_n and F'_t can be obtained as;

$$F_n = F_n' \cos(\beta_g + \psi) - F'_t \sin(\beta_g + \psi) \quad (14)$$

$$F_t = F_n' \sin(\beta_g + \psi) + F'_t \cos(\beta_g + \psi) \quad (15)$$

The defections δ_n and δ_t in the normal and tangential directions, respectively, can be obtained as follows,

$$\delta_n = F_n / K_{eq} \quad (16)$$

$$\delta_t = F_t / K_{eq} \quad (17)$$

where K_{eq} is the dynamic grinding coefficient and is a function of the work piece stiffness, K_w, grinding wheel stiffness, K_g and machine stiffness, K_m. The relationship between F'_n and F'_t is referred to as the coefficient of grinding, i.e., μ, (Ioan 2007).

$$\mu = \frac{F_t}{F_n} \quad (18)$$

The deflection δ is given by,

$$\delta = \delta_n \sqrt{1 + \mu^2} \quad (19)$$

The deflections are computed as a function of time.

4. Prediction of chattervibrations

A computer program was used to solve equations 16 and 17 for the normal and tangential displacements. The parameters used in the analysis are as shown in Table 1. A coefficient of grinding of 0.5 is used (for steel), grit density of 9.5 (for the CBN wheel used) and a uniform grit shape factor of 1 assumed. The flowchart for the computations is shown in Figure 3.

5. Experimental setup

In order to test the effectiveness of the proposed model in predicting vibration in grinding, measurement of vibration in cylindrical plunge grinding process was carried out with different sets of parameters for mild steel (0.2% C). The focus was on the amplitudes and modes of the vibrations.

The experiments were carried out using a universal HIGH-GLOSS 450-H grinding machine manufactured by Kondo Machine Works. The machine has a spindle rotational speed of 1430 rpm and work piece rotational speeds that can be set at 55 rpm, 130 rpm, 215 rpm or 295 rpm. It has a provision for feeding in two orthogonal axes, that is X and Y, and can be automatically fed in the X direction only. It has a resolution of 0.01 mm in the feed direction. A B126 Cubic Boron Nitride (CBN) wheel with a grit density of 9.5/mm^2, outer diameter of 405 mm, inner diameter of 203 mm and thickness of 75 mm was used. A contact type displacement sensor, DT-10D, with a range of 10 mm and a piezo-electric tool dynamometer (AST-MH) were used for displacement and force measurements, respectively.

Since the grinding wheel speed is constant at 1430 rpm, there was need to vary the spindle speed by use of an external means. A variable frequency drive (Powerflex4 from Allen Bradley) was used to adjust the speed of the grinding wheel by controlling the speed of the spindle motor. The experimental setup was as shown in Figure 4.

6. Results and discussion

6.1 Model validation

The predicted and measured displacements as well as power spectra for the corresponding vibrations are shown in Figures 5 through 7. The root mean square (rms) values of work piece displacements were taken as indicative of the amplitudes of vibration and the vibration frequencies were obtained from power spectra. The rms values and the power spectra were obtained using MATLAB software.

From the power spectral analysis it can be seen that, there are more vibration modes during the grinding process, than in the model predictions. This could be attributed to vibrations of the machine structure which was not considered in the model.

It can be seen that in all cases, the predicted values at lower grinding wheel speeds are closer to the experimental values than at higher speeds. This could be due to the fact that, while grinding at high speeds, there is generation of higher temperatures which contribute to higher grit breakage. Temperature T, at the contact surface in grinding has been shown to have the following relationship (Clarence 2005).

$$T \alpha \sqrt{a_e . v_s . C . r}$$

in this equation, a_e is the depth of cut (the depth of work material removed per revolution), v_s is the surface velocity of the grinding wheel, C is the active grit density and r is the grit cutting point shape factor. This effect was not accounted for in the model.

6.1.1 Effect of variation of work piece speed on vibration amplitudes

The work piece speed was varied in order to investigate the effect of variation of work piece speed on the vibration amplitudes at grinding wheel speed of 1430 rpm and an in-feed of 0.05mm. The results are as shown in Figure 8. In this figure the variation of the predicted values of vibration from the measured values is within ±0.03 µm, except at work piece speed of 295 rpm, where the predicted value is more than the measured value with a ±0.05 µm. It can also be seen that, the lowest values of the vibration amplitudes are obtained at a work piece speed of and 55 rpm, while the highest predicted and measured values of the displacement are at work piece speeds of 295 rpm and 130 rpm, respectively.

6.1.2 Effect of variation of wheel speed on vibration amplitudes

Analysis on the effect of variation of wheel speed on amplitudes of vibration shows similar results as for the effect of the variation of work piece speed for grinding mild steel, that is, non-linear relationship between the amplitudes of vibration and the wheel speed as shown in Figure 9. From the figure, the variation of the predicted displacements from the measured values is within ±0:03 µm range except at a wheel speed of 1430 rpm, where the predicted value is more than the measured value with ±0:05 µm. It is also seen on this figure that, the lowest values of the vibration amplitudes (displacements) are obtained at grinding wheel speed of 700 rpm, while the highest predicted and measured values of displacements are at wheel speeds of 1200 rpm and 500 rpm, respectively.

6.1.3 Effect of variation of in-feed on vibration amplitudes

The in-feed was varied with the work piece and wheel speed at 295 rpm and 1430 rpm, respectively, in order to investigate the effect of variation of in-feed on the vibration amplitudes. The predicted and measured values of displacement indicate that, vibration amplitudes increase nonlinearly with in-feed. From Figure 10, the highest value of the displacement occur at in-feed of 0.07 mm and the lowest occur at in-feed of 0.01 mm in grinding mild steel.

Also, the variation of the predicted values from the measured values is within a ±0.03 µm range.

From the three cases considered above, it can be seen that, the model predictions vary from the measured values with up to a maximum of 0.05 µm.

7. Conclusion

A dynamic model for prediction of chatter vibration in cylindrical plunge grinding process has been developed. This model predicts displacements at different grinding wheel and work piece speeds as well as in-feeds. From the power spectral analysis, it was seen that there were several modes of vibration present during the grinding process. It was shown that, variation in grinding wheel and work piece speeds, and in-feed result in change in the vibration modes and amplitudes of vibration.

References

Biera J., Vinolas J., Nieto F., (1997), Time-domain dynamic modeling of external plunge grinding process, *International Journal of Machine Tools and Manufacture*, 37, 1555–1572.

Clarence W.S., (2005), *Vibration and Shock Handbook*, CRC Press, Taylor & Francis Group.

Daniel P., (1999), Modeling and simulation of grinding processes, *in Annals of the Oradea University, Fascicle of Management and Technological Engineering*.

Orynski F., Pawlowski W., (1999), The influence of grinding process on forced vibration damping in headstock of grinding wheel of cylindrical grinder, *International Journal of Machine Tools and Manufacture*, 39, 229–235.

Garitaonandia I., Fernandes M. H., Albizuri J., Hernandez J. M. and Barrenetxea D., (2010), A new perspective on the stability study of centerless grinding process, *International Journal of Machine Tools and Manufacture*, 50, 165–173.

Hahn H. and Robert S. K., (1986), *Handbook of modern grinding technology*, Chapman and Hall (New York).

Hongqi L. and. Shin Y. C., (2007), A study on chatter boundaries of cylindrical plunge grinding with process condition dependent dynamics, *International Journal of Machine Tools and Manufacture*, 47, 1563–1572.

Huang-Cheng C. and Wang J., (2008), A stochastic grinding force model considering random grit distribution, *International Journal of Machine Tools and Manufacture*, 48, 1335–1344.

Ichiro I., (2008), Performance enhancement of grinding processes - Mutual interaction between the material removal processes and the machine tool, *JKET Engineering Journal, English Edition*, 1004E, 3–8.

lnasaki I., Karpuschewski B. and Lee H. S., (1999), Grinding Chatter - Origin and Suppression, *Journal of Machine Tools and Manufacture*, 4, 25–32.

Ioan D. M., Mike H., Eckart U., Rowe W.B. and Ichiro I., (2007), *Handbook of Machining with Grinding Wheels*, CRC Press, Taylor and Francis Group.

Junkar M. and Filipic B., (2001), Grinding process control through monitoring and machine learning, *IEEE*, 4, 77–80.

Kuang-Hua F. and Shuh-Bin W., (1997), Force modeling and forecasting in creep feed grinding using improved back propagation (BP) neural network," *International Journal of Machine Tools and Manufacture*, 37, 1167–1178.

Lizarralde R., Montejo M., Barrenetxea D., Marquinez J.I. and Gallego I., (2006), Intelligent Grinding: Sensorless instabilities detection, *IEEE Instrumentation & Measurement Magazine*, 6, 30–37.

Merchant M.E. (1945), Mechanics of the metal cutting process, *Journal of applied physics*, 16, 267–275.

Mohammed A. and Abdallah E., (2000), Effect of grinding forces on the vibration of grinding machine spindle system, *International Journal of Machine Tools & Manufacture*, 40, 2003–2030.

Orynski F. and Pawlowski W., (2002), The mathematical description of dynamics of the cylindrical grinder, *International Journal of Machine Tools and Manufacture*, 42, 773–780.

Piotr S., (2007), Grinding forces in regular surface texture generation, *International Journal of Machine Tools and Manufacture*, 47, 2098–2110.

Rogelio H. and Steven L., (2006), Plunge grinding process surface roughness model and process control. *Georgia Institute of Technology.*

Sakakura M., Tsukamoto S., Fujiwara T. and Inasaki I., (2004), Visual simulation of grinding process, *IEEE*, 1, 233–239.

Yi L., Gracewski S. M., Funkenbusch P. D. and Ruckman J., (2000), Chatter simulation and stability predictions for contour grinding of optical glasses, *Optical Society of America*, 204-2011.

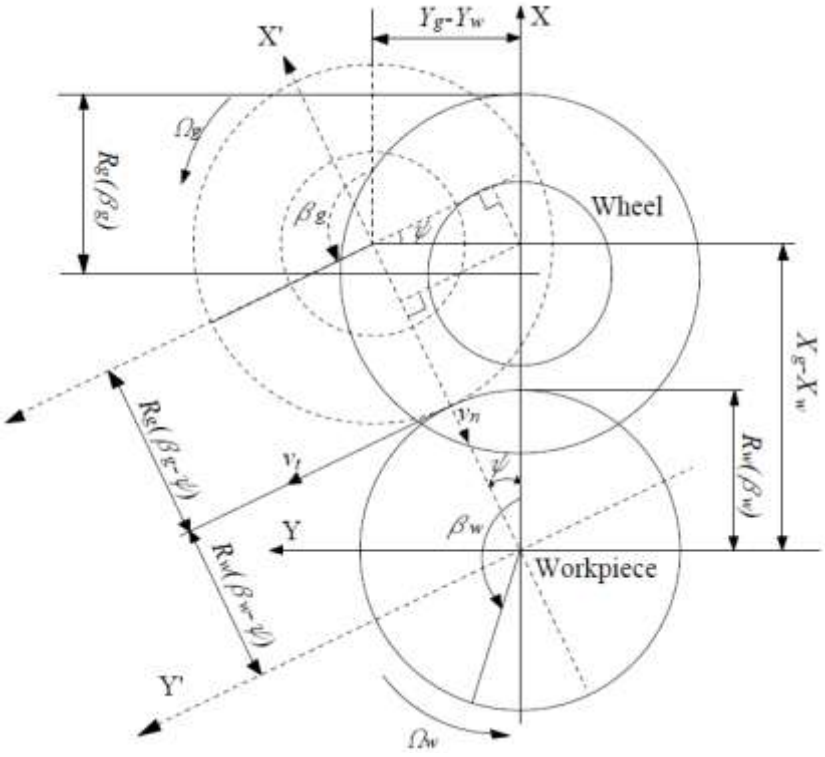

Figure 1: Kinematics of a plunge grinding process, Hongqi and Shin (2007).

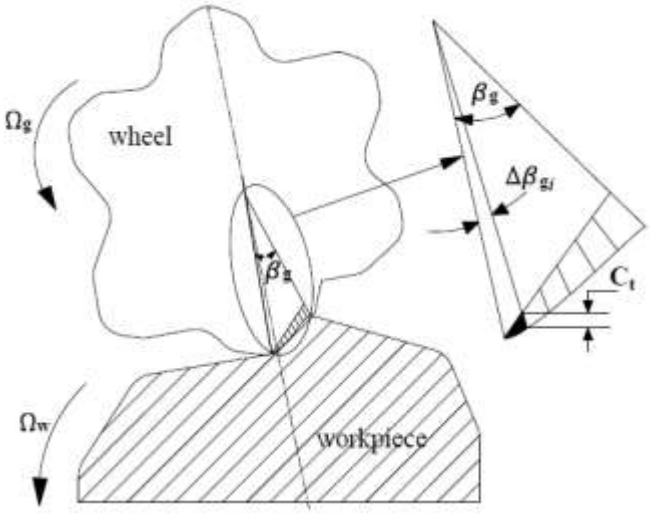

Figure 2: Geometrical interaction between wheel and work piece.

Table 1: Grinding parameters

Parameter	**Value**
Active grit density (C)	9.5
Coefficient of grinding (μ)	0.5
Grit shape factor (r)	1
Grinding wheel diameter	405 mm
Work piece diameter	30 mm

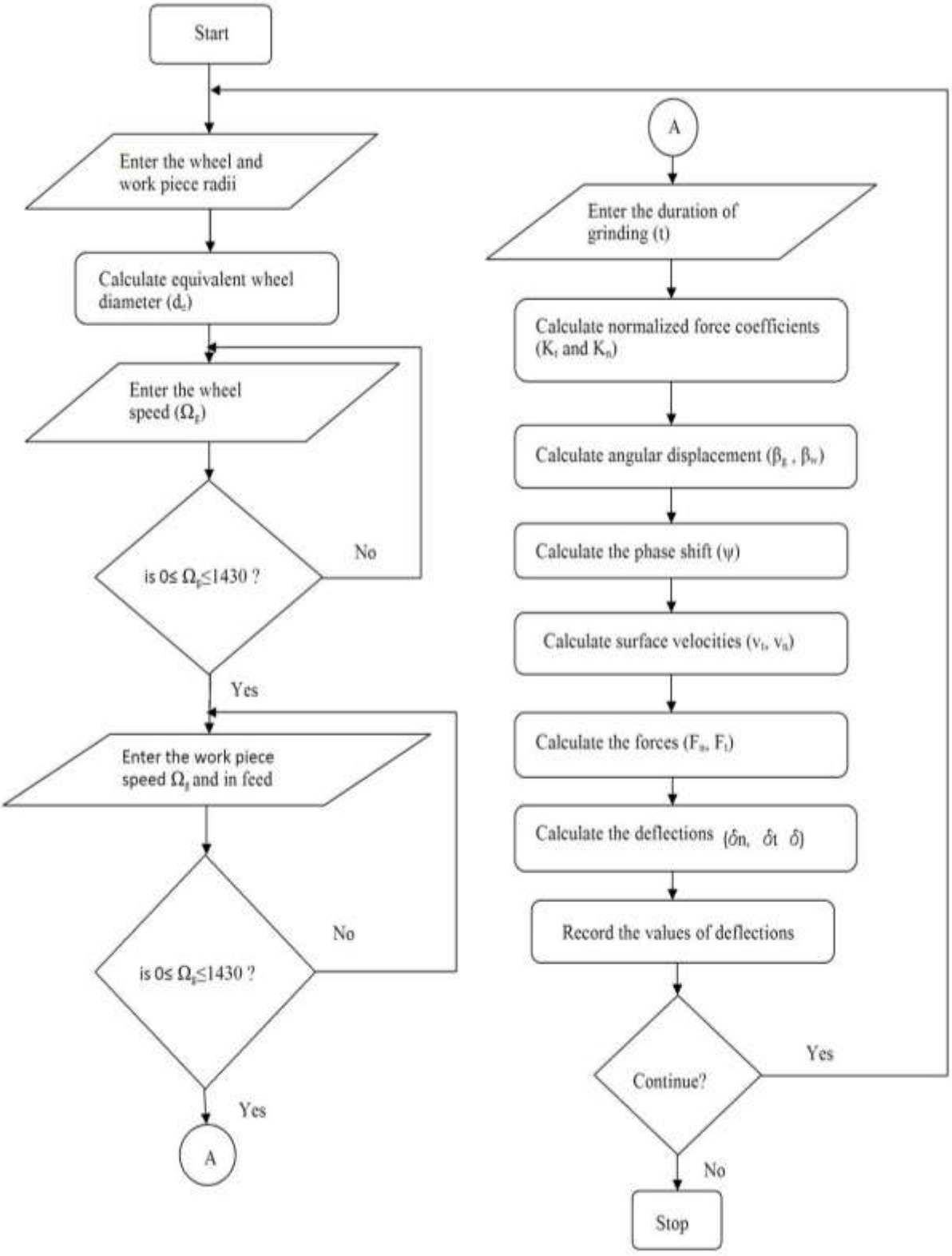

Figure 3: Flowchart for the execution of the simulation program.

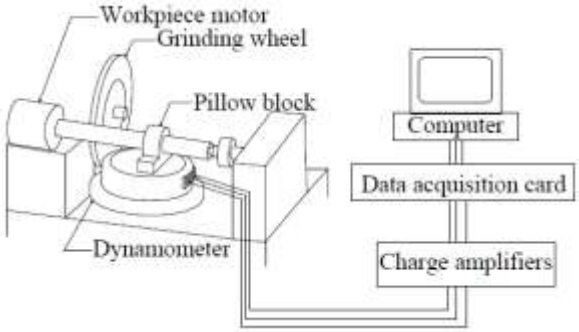

Figure 4: Experimental setup for measurement of grinding vibrations.

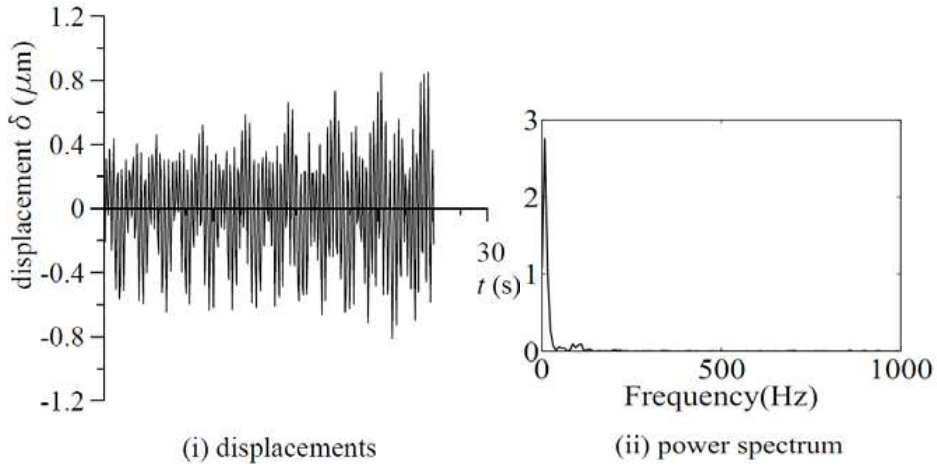

(a) Predicted displacements: the rms value is 0.2689

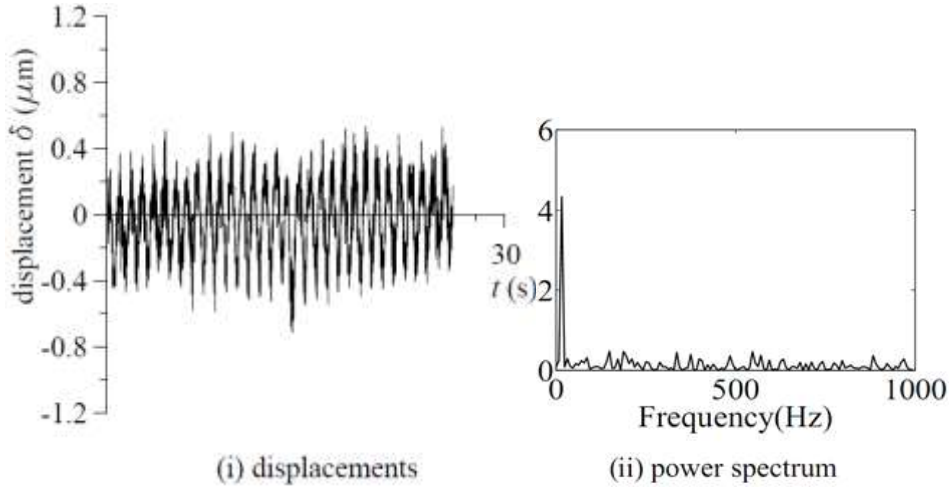

(b) Measured displacements: the rms value is 0.2199

Figure 5: Vibrations in grinding (grinding wheel speed, 1430 rpm; work piece speed, 295 rpm)

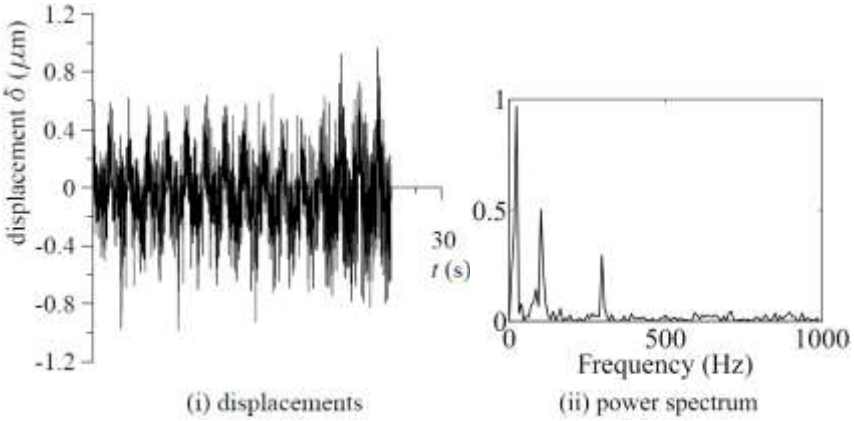

(a) Predicted displacement: the rms value is 0.2635

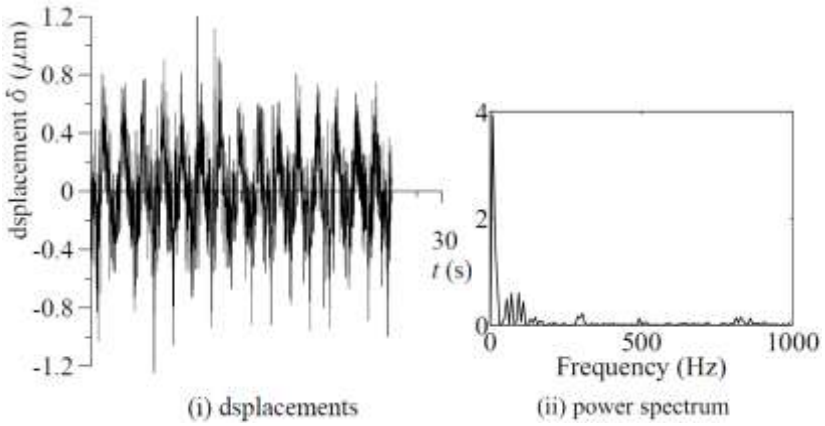

(b) Measured displacements: the rms value is 0.2941

Figure 6: Vibrations in grinding (wheel speed, 500 rpm; work piece speed, 295 rpm)

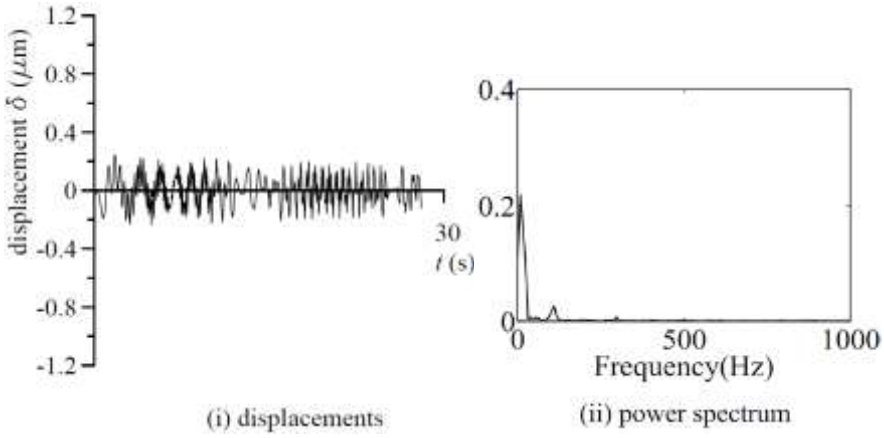

(a) Predicted displacements: the rms value is 0.1039

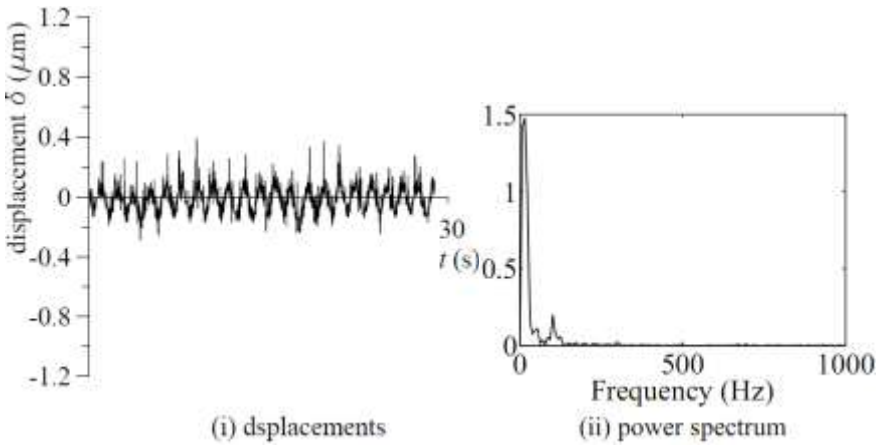

(b) Measured displacements: the rms value is 0.0824

Figure 7: Vibrations in grinding (grinding wheel speed, 700 rpm; work piece speed, 295 rpm)

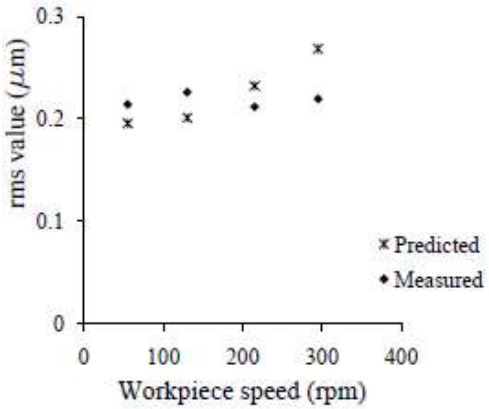

Figure 8: Variation of rms values of displacements with work piece speed in grinding (wheel speed, 1430 rpm).

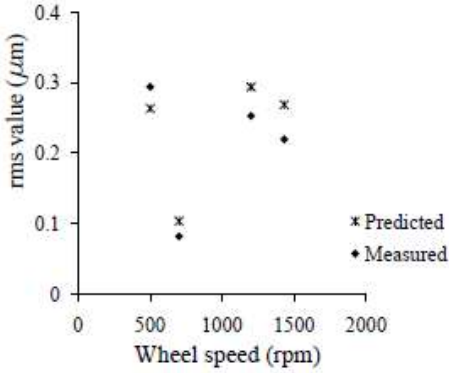

Figure 9: Variation of rms values of displacements with wheel speed in grinding (work piece speed, 130 rpm)

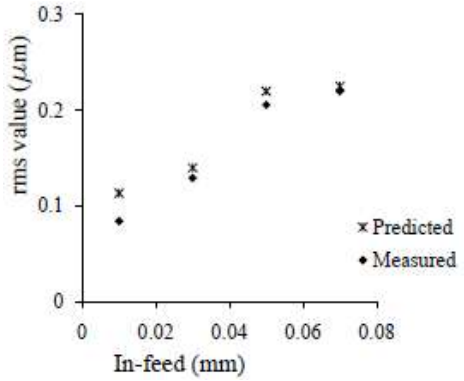

Figure 10: Variation of rms values of displacements with in-feed